International Journal of Heat and Mass Transfer 60 (2013) 241–251

Contents lists available at SciVerse ScienceDirect

International Journal of Heat and Mass Transfer

journal homepage: www.elsevier.com/locate/ijhmt

Parametric study and field synergy principle analysis of H-type finned tube bank with 10 rows

Yu Jin, Gui-Hua Tang, Ya-Ling He, Wen-Quan Tao *

Key Laboratory of Thermo Fluid Science & Engineering, School of Energy and Power Engineering, Xi'an Jiaotong University, Xi'an, Shannxi 710049, China

ARTICLE INFO

Article history:
Received 16 May 2012
Received in revised form 13 November 2012
Accepted 14 November 2012
Available online 1 February 2013

Keywords:
Waste heat recovery
H-type finned tube
Heat transfer
Pressure drop
Parametric study
Field synergy principle
Numerical simulation

ABSTRACT

In this paper, three-dimensional numerical studies are performed for heat transfer and pressure drop characteristics of H-type finned tube bank with 10 rows by software FLUENT. The effects of seven geometric parameters (tube row number, fin thickness, slit width, fin height, fin pitch, spanwise tube pitch and longitudinal tube pitch) and Reynolds number are examined. It is found that for the tube bundle studied, the heat transfer and fluid flow are in the developing region, and they become periodically fully developed after the 10th row. Among the seven geometric parameters spanwise tube pitch has the most important effect and slit width has the least important effect, with other five parameters in between. The results are also analyzed from the view point of field synergy principle. It is found that the effects of the eight parameters on heat transfer and fluid flow characteristics can be well described by the field synergy principle. Correlations of *Nu* and *Eu* for the 10-row tube bundle are presented.

1. Introduction

In order to improve the thermal performance of heat exchangers, it is necessary to enhance heat transfer on the side of heat exchanger where the thermal resistance is dominant in the overall heat transfer process. The extended surface has been proved to be an effective method for enhancing gas-side heat transfer. Fin-and-tube heat exchangers are the typical equipment with extended surface and widely used in many engineering applications, such as air conditioning units, compressor intercoolers, boiler economizers, etc.

A lot of experimental and numerical studies have been conducted on airside heat transfer performances of fin-and-tube heat exchangers. A brief review is presented below. Wang et al. [1–6] made extensive experiments on heat transfer and pressure drop characteristics of wavy fin-and-tube heat exchangers. Madi et al. [7] investigated the effects of fin thickness, fin pitch and the number of tube rows on the airside performance of wavy fin-and-tube heat exchangers. Halici et al. [8] experimentally investigated the effect of the number of tube rows on the heat transfer, mass transfer and fluid flow characteristics of plain fin-and-tube heat exchangers. Lozza and Merlo [9] performed the heat transfer measurements of the plate fin, the wavy fin and the louvered fin in the Luve Contardo experimental facilities. Mon and Gross [10] investigated the effects of the fin spacing on four-row annular-finned tube bundles in staggered and in-line arrangements by three-dimensional numerical study. Cheng et al. [11] numerical designed slotted fin surface with field synergy principle. Qu et al. [12] studied three-dimensional strip fin surfaces with X-arrangement. He et al. [13] presented a three-dimensional numerical simulation to study the heat transfer and fluid flow characteristics of the plain fin-and-tube heat exchangers in laminar flow. The effects of Reynolds number, fin pitch, the number of tube rows, the spanwise pitch and the longitudinal pitch on finned tube heat exchangers were analyzed. Zhou and Tao [14] studied the strip fin with radial strips. Tao et al. [15] and Jin et al. [16] made an optimized design of two-row slotted fin surface with X-shape strip arrangement. Tao et al. [17] studied the laminar heat transfer and fluid flow characteristics of wavy fin heat exchangers with elliptic/circular tubes. The results were also analyzed from the view point of field synergy principle. Xie et al. [18] numerically studied the airside laminar heat transfer and fluid flow characteristics of plain fin-and-tube heat exchangers with large number of large-diameter tube rows. The effects of Reynolds number, the number of tube rows, tube diameter, tube pitch, fin pitch and fin materials were examined. The above-mentioned different kinds of fin-and-tube heat transfer surfaces usually have small pitches between two adjacent fins and are mainly used in air conditioning industry because air is a clean working medium.

* Corresponding author. Tel./fax: +86 029 82669106.
E-mail address: wqtao@mail.xjtu.edu.cn (W.-Q. Tao).

0017-9310/$ - see front matter
http://dx.doi.org/10.1016/j.ijheatmasstransfer.2012.11.043

Nomenclature

A	area, m^2
$C_{1\varepsilon}C_{2\varepsilon}C_{\mu}$	turbulence model constants
c_p	specific heat, J kg^{-1} K^{-1}
D	tube outside diameter, m
Eu	Euler number
Fp	fin pitch, m
Ft	fin thickness, m
h	heat transfer coefficient, W m^{-2} K^{-1}
H	fin height, m
k	turbulent kinetic energy, m^2 s^{-2}
Nu	average Nusselt number
p	pressure, Pa
Pr	Prandtl number
P	pumping power, W
Δp	pressure drop, Pa
Re	Reynolds number
S_1	spanwise tube pitch, m
S_2	longitudinal tube pitch, m
S	modulus of the mass rate-of-stress tensor, s^{-1}
S_{ij}	mean stress rate, s^{-1}
T	temperature, K
ΔT	the log mean temperature difference, K
u	velocity, m s^{-1}
W	slit width, m

Greek symbols

Φ	heat transfer rate, W
λ	thermal conductivity, W m^{-1} K^{-1}
μ	viscosity, kg m^{-1} s^{-1}
ν	kinematic viscosity, m^2 s^{-1}
ρ	density, kg m^{-3}
β	local intersection angle, Deg.
ε	turbulent energy dissipation rate, m^2 s^{-3}

Subscripts

in	inlet
out	outlet
max	maximum
up	upstream
w	wall
eff	effective

For industrial gases, such as gas of a boiler furnace and discharged gases from many engineering furnaces, discrete fins with rectangular shape are often used to enhance the gas convective heat transfer. In recent years, with the developments in manufacturing techniques, the configurations of fins become more complicated, among which are the widely used H-type finned tubes in boiler economizer. H-type finned tube as shown in Fig. 1 is derived, in large part, from the rectangle-type finned tube. Because of its unique groove structure in fin surface, H-type finned tube has excellent anti-wear and anti-fouling performance, which is of great importance for the application in the heat exchangers of waste heat recovery. In addition, some heat transfer areas of the fin in the separation zone are removed to reduce the negative effect on heat transfer. Liu et al. [19] conducted experimental study on the characteristics of heat transfer and fluid flow for H-type finned tube. Yu et al. [20] performed experimental tests to study the heat transfer and flow resistance characteristics at air-side of single or double H-type finned tube banks. The flow and temperature fields were also obtained by numerical simulation and the results agreed well with that of their experimental test. Zhang et al. [21] carried

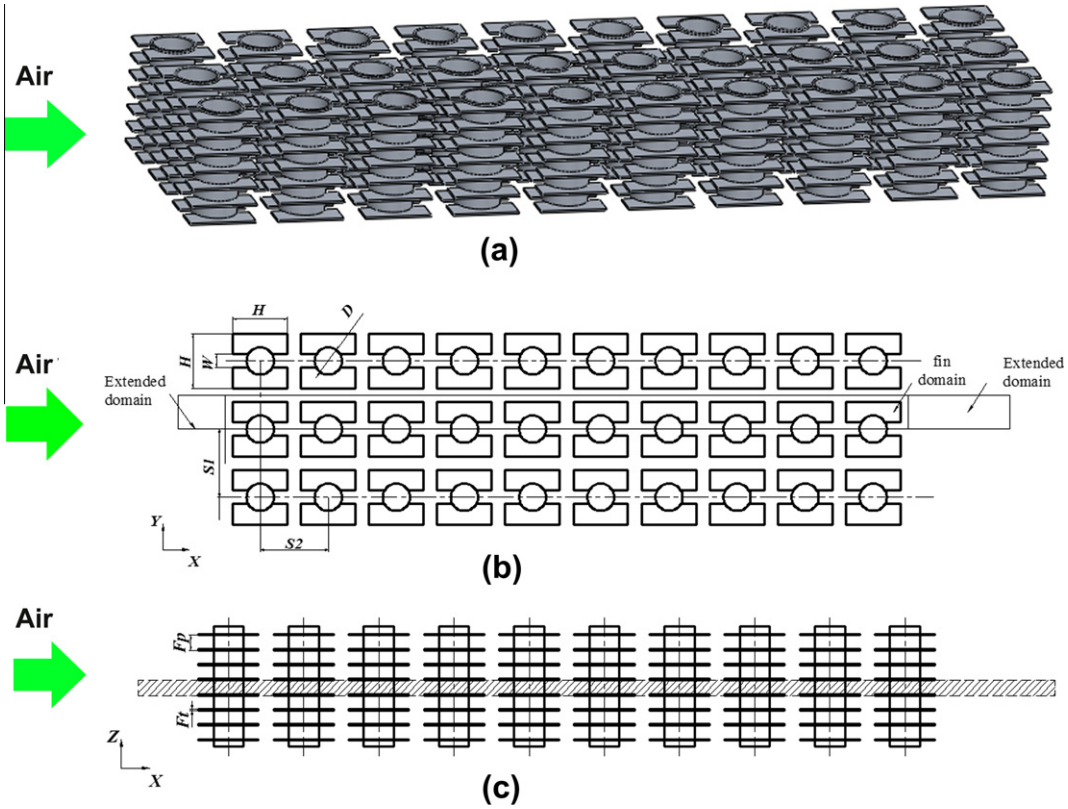

Fig. 1. Schematic configuration of an H-type finned tube heat transfer surface.

out numerical simulation on heat transfer characteristics of H-type finned tube. The effects of the number of tube rows and longitudinal space on heat transfer coefficient were also analyzed. However, so far no systematic study has been conducted for the effects of geometric parameters on heat transfer and pressure drop characteristics of H-type finned tube.

As far as the mechanism of heat transfer enhancement is concerned, in 1998, Guo et al. [22] proposed a novel concept about the enhancement of convective heat transfer for parabolic flow and showed that the reduction of the intersection angle between the velocity and temperature gradient can effectively enhance the heat transfer. This concept is now called as field synergy principle. A lot of experimental and numerical studies [23–29] have been conducted, showing that the field synergy principle could well explain the mechanism of the convective heat transfer enhancement. The examples in the above mentioned references are all in laminar flow. Zeng and Tao [30] demonstrated that the field synergy principle is also valid for turbulent flow. In order to shorten the length of the article, the detail content of the field synergy principle which can be found in above mentioned references, is not presented here.

In this paper, numerical study of an H-type finned tube surfaces is performed. The effects of eight parameters: number of tube rows, fin thickness, slit width, fin height, fin pitch, spanwise tube pitch, longitudinal tube pitch and Reynolds number on heat transfer and fluid flow characteristics are examined. The results are explained from the view point of the field synergy principle.

In the following passage, the geometric model and the computational domain of the studied H-type fin will firstly be provided with adopted turbulence model and boundary conditions. Then the definitions of the studied parameters are offered. Model validation and parameter effects of numerical results are presented in details in the results and discussion part. Finally some conclusions are made.

2. Model description and numerical method

2.1. Physical model

A schematic diagram of an H-type multiple-row finned tube heat transfer surface is shown in Fig. 1. The geometric parameters of the basic H-type finned tube are listed in Table 1. Fig. 1(b) gives a top view of the computation domain of the 10-row H-type finned tube. Fig. 1(c) presents the side view of the computational domain shown by the shaded area, and its top and bottom are the symmetrical lines of the two neighboring fins.

2.2. Governing equations and boundary conditions

The fluid is assumed to be incompressible with constant property and the gas flow is in turbulence and steady condition. Due to the relatively larger heat transfer coefficient between the cooling water and inner wall of the tube and the large thermal conductivity of the tube wall, the tube is assumed to be at constant temperature. However, the temperature distribution in the fin surface has to be calculated. Therefore, the computations are of conjugated type, in which both the temperature in the solid fin surface and in the fluid is to be determined simultaneously [31]. The tubes and fins are made of carbon steel with constant thermal conductivity.

The governing equations in Cartesian coordinates include mass, momentum and energy conservation equations. They can be found in many references and are not presented here for simplicity. Only the turbulence model is presented below.

The RNG $k-\varepsilon$ turbulence model [32] is adopted:

$$\rho\frac{Dk}{Dt}=\frac{\partial}{\partial x_i}\left[\alpha_p\mu_{\text{eff}}\frac{\partial k}{\partial x_i}\right]+\mu_t S^2-\rho\varepsilon \tag{1}$$

Table 1
Geometric parameters of the basic H-type finned tube in physical model.

H/mm	W/mm	Fp/mm	Ft/mm	D/mm	S_1/mm	S_2/mm	N
73.4	15	16.875	2.5	38	108	120	10

$$\rho\frac{D\varepsilon}{Dt}=\frac{\partial}{\partial x_i}\left[\alpha_p\mu_{\text{eff}}\frac{\partial \varepsilon}{\partial x_i}\right]+C_{1\varepsilon}\frac{\varepsilon}{k}\mu_t S^2-C_{2\varepsilon}\rho\frac{\varepsilon^2}{k}-R \tag{2}$$

where effective viscosity $\mu_{\text{eff}}=\mu+\mu_t$, and $\mu_t=\rho C_\mu\frac{k^2}{\varepsilon}$ with $C_\mu=0.0845$. R is the rate of strain term given by

$$R=\frac{C_\mu\rho\eta^3(1-\eta/\eta_0)}{1+\beta\eta^3}\frac{\varepsilon^2}{k} \tag{3}$$

where $\eta=sk/\varepsilon$, $\eta_0=4.38$, $\beta=0.012$ and $S^2=2S_{ij}S_{ij}$ is the modulus of the rate of strain tensor expressed as $S_{ij}=\frac{1}{2}\left(\frac{\partial u_i}{\partial x_j}+\frac{\partial u_j}{\partial x_i}\right)$. The RNG model gives $C_{1\varepsilon}=1.42$ and $C_{2\varepsilon}=1.68$.

In order to ensure the inlet uniformity, the computational domain is extended upstreamly by five times of the original heat transfer zone for the entrance section. At the exit of heat transfer region, the domain was extended by 10 times of the original heat transfer zone in order to make sure that the local one-way method can be used for the numerical treatment at the domain outlet.

The computational domain includes six boundaries: inlet, outlet and four symmetrical boundary surfaces (top, bottom, front and back). At the inlet boundary, dry air entering the computational domain is assumed to have uniform velocity u_{in}, temperature T_{in} (420 K) and the turbulent intensity I (5%) with the velocity components in the y and z directions being zero. The fluid region is comprised of the inlet, outlet and bundle zone and the solid region includes the fin. At the solid surfaces, no-slip conditions for the velocity are specified. Heat convection to the fin and heat conduction in the fin is considered. At the tube surface constant temperature T_{w} (360 K) is assigned. At the symmetry planes, heat flux is assumed zero. At the fluid symmetry plane the normal velocity component and the normal first derivatives of other variables are zero, while at the solid symmetry plane all velocity components and the normal first derivative of temperature are zero.

A three-dimensional and steady-state numerical simulation was conducted by using the commercial software FLUENT [33] with a second-order discretization scheme for both convective and diffusive terms. When the residual of each variable is less than 1.0×10^{-5}, the numerical computation is regarded converged.

2.3. Parameter definition

In the numerical data reduction, the following characteristic and non-dimensional parameters are introduced.

$$Re=\frac{\rho u_{\text{in}}D}{\mu} \tag{4}$$

$$Nu=\frac{hD}{\lambda} \tag{5}$$

$$\dot{\Phi}=\dot{H}_{\text{out}}-\dot{H}_{\text{in}} \tag{6}$$

$$Eu=\frac{2\Delta p}{\rho u_{\text{in}}^2 N} \tag{7}$$

$$\Delta p=p_{\text{in}}-p_{\text{out}} \tag{8}$$

$$\Delta T=\frac{(T_{\text{out}}-T_{\text{w}})-(T_{\text{in}}-T_{\text{w}})}{\ln\left(\frac{T_{\text{out}}-T_{\text{w}}}{T_{\text{in}}-T_{\text{w}}}\right)} \tag{9}$$

$$h=\frac{\dot{\Phi}}{A\Delta T} \tag{10}$$

$$P=\Delta p u_{\text{in}}A_{\text{f}} \tag{11}$$

In the above equations, u_{in} is the average oncoming flow velocity. $\dot{H}_{in}$ and $\dot{H}_{out}$ are the fluid enthalpy rates of inlet and outlet positions of the computational domain. p_{in} and p_{out} are the bulk pressure at inlet and outlet section of fin surfaces respectively. A_f is the frontal area. A is the total air side heat transfer area (both tube and fin surface). T_w is the average temperature of total air side heat transfer area. u_c is the air velocity in the minimum flow cross-section of the tube row. P is the pumping power.

To analyze the heat transfer and the fluid flow characteristics of H-type finned tube from the view point of field synergy principle, the local intersection angle between the velocity and temperature gradient is determined as follow.

$$\beta = \arccos \frac{u \cdot \frac{\partial T}{\partial x} + v \cdot \frac{\partial T}{\partial y} + w \cdot \frac{\partial T}{\partial z}}{|\vec{U}| \cdot |\nabla T|} \tag{12}$$

And the module-averaged synergy angle of the computation domain of the fin area can be obtained by using numerical integration,

$$\beta_m = \arccos \frac{\sum |\vec{U}|_i \cdot |\nabla T|_i \cdot \cos \beta_i \cdot dv_i}{\sum |\vec{U}|_i \cdot |\nabla T|_i \cdot dv_i} \tag{13}$$

Here dv_i is the volume element of the control volume. It is interesting to note that there are several average schemes from local synergy angle to the domain average synergy angle, including arithmetic mean, volume weight mean, and module-volume weight average mean [34]. And it was shown that even though the absolute values of different definitions are different the variation trends of different definitions are the same. And it is the variation trend that is used to guide our analysis. However, according to the full understanding of the field synergy principle shown in [23], the module-volume weight average mean is the most appropriate one in which the effects of local $|U|$,$|\nabla T|$, synergy angle and volume are all reflected. Hence, this definition is adopted here for comparison.

2.4. Grid independent solution

In order to validate the grid-independency of the solution, five different grid systems are investigated, including about 160 000, 403 000, 807 000, 1 371 000 and 1 843 000 cells. The predicted average *Nu* numbers of the whole tube bundle from the five grid systems are shown in Fig. 2, from which we can see that the solution of the grid system of 1 371 000 can be regarded grid-independent. This grid system is adopted in our computation.

2.5. Validation of the computational model

In order to validate the reliability of the computational model and numerical method, numerical simulation is carried out for the H-type finned tube heat transfer surface. The geometric parameters for the H-type finned tube are shown in Table 2, which are taken from Ref. [19]. The average air velocity ranges from 1 m/s to 10 m/s and the corresponding *Re* number ranges from 3834 to 33 072. The predicted Nusselt number and Euler number are compared with the corresponding experimental correlations established by Liu et al. [19] as shown in Fig. 3. For the readers' convenience, the correlation of the average *Nu* number and Euler number are presented as Eqs. (14) and (15) respectively. From Fig. 3, the maximum deviation in the Nusselt number and Euler number are less than 9.5% with the average deviation being around 6.5%. The good agreement between the simulation results and tested results indicates that the numerical model is reliable.

$$Nu = 0.09152 Re^{0.7013} Pr^{0.33} \tag{14}$$

$$Eu = 0.2963 Re^{-0.0449} \tag{15}$$

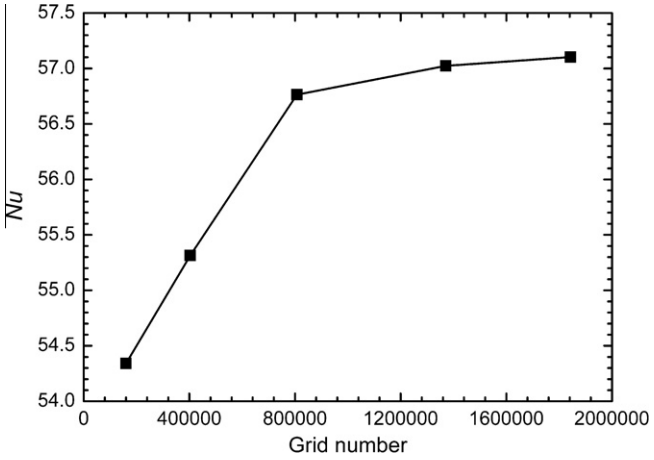

Fig. 2. Variation of the predicted *Nu* number with grid number systems.

Table 2
Geometric parameters of the H-type finned tube for model validation.

H/mm	*W*/mm	*Fp*/mm	*Ft*/mm	*D*/mm	S_1/mm	S_2/mm	*N*
84	15	20	2	38	90	90	10

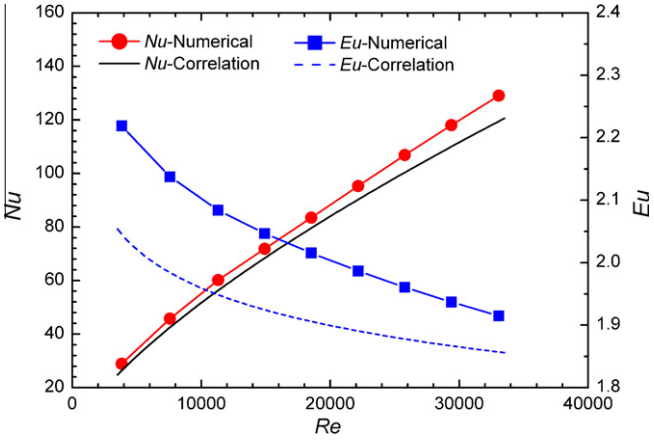

Fig. 3. Correlation-numerical comparison of *Nu* number and *Eu* number for model validation.

3. Numerical results and discussion

In the following passage, the comparison between rectangle fin and H-type fin is first analyzed, followed by the effects of number of tube rows, fin thickness, slit width, fin height, fin pitch, spanwise tube pitch and longitudinal tube pitch and Reynolds number on heat transfer and fluid flow respectively. Then the simulation results are discussed and analyzed from the view point of field synergy principle.

3.1. Comparison between rectangle-type finned tubes with H-type finned tube

H-type finned tube is mainly derived from the rectangle-type finned tube. So this paper first briefly compares H-type finned tube with the rectangle-type finned tube. Fig. 4(a) presents the variation of heat transfer rate versus *Re* number for the rectangle-type tube and H-type finned tube, respectively. From Fig. 4(a), we can see

that the heat transfer rate of rectangle-type tube is a bit larger than H-type finned tube, since the heat transfer area of the rectangle-type finned tube is a bit larger than that of H-type finned tube. Fig. 4(b) shows the relations between *Nu* number and *Re* number of rectangle-type tube and H-type finned tube. We can see that the *Nu* number of H-type finned tube is a bit larger than that of rectangle-type finned tube, due to the removing of some heat transfer area in the separation zone. In Fig. 4(c), the variation of the pressure drop versus *Re* number is presented. Because the surface area of the H-type finned tube is a bit smaller than that of the rectangle-type finned tube, the pressure drop of the H-type finned tube is lower than that of the rectangle-type finned tube. Fig. 4(d) shows that heat transfer rate per pumping power of the rectangle-type finned tube is a bit higher than that of H-type finned tube. It is worth noting that in this paper, the medium is clean air, so the effects of wear and fouling of heat transfer surface on heat transfer and fluid flow are not considered. Because of the unique groove structure in fin surface, H-type finned tube has excellent anti-wear and anti-fouling performance, which makes H-type finned tube more appropriate used with industry gas.

3.2. The effect of number of tube rows

For examining the effect of number of tube rows on the heat transfer and fluid flow, in the simulation the number of tube rows varied from 1 to 10. The other parameters remained the same as H-type finned tube defined in the physical model. The Reynolds number was taken as 1.5×10^4. It may be noted here that in the following presentation of numerical results for examining the effects of geometric parameters, the numerical studies were always conducted for $Re = 1.5 \times 10^4$ and with one parameter varying in a certain range and the other parameters remained the same as H-type finned tube defined in the physical model. In addition all non-dimensional geometric parameters were based on the tube outside diameter. For the simplicity of presentation this will not be restated anymore.

Fig. 5 shows the effects of number of tube rows on bundle average Nusselt number, intersection angle, pressure drop, Euler number, heat transfer rate per unit frontal area and heat transfer rate per pumping power. The total pressure drop and the heat transfer rate per unit frontal area both increase with the tube number obviously, and the increasing trends are gradually weakened. The character of gradually weakening with tube number of the heat transfer rate is caused by the fact that the local *Nu* number decreases with the increase of the number of tube rows, while this variation character of the pressure drop leads to the descending variation of the per row Euler number with tube row number. The increase of average synergy angle with tube number is consistent with the Nusselt number variation. The heat transfer rate per unit pumping power increases with the increase of the tube row number which is due to the fact that with the increase of tube row number the positive effect of the total heat transfer rate increase is much larger than the negative effect of the total pressure drop increase.

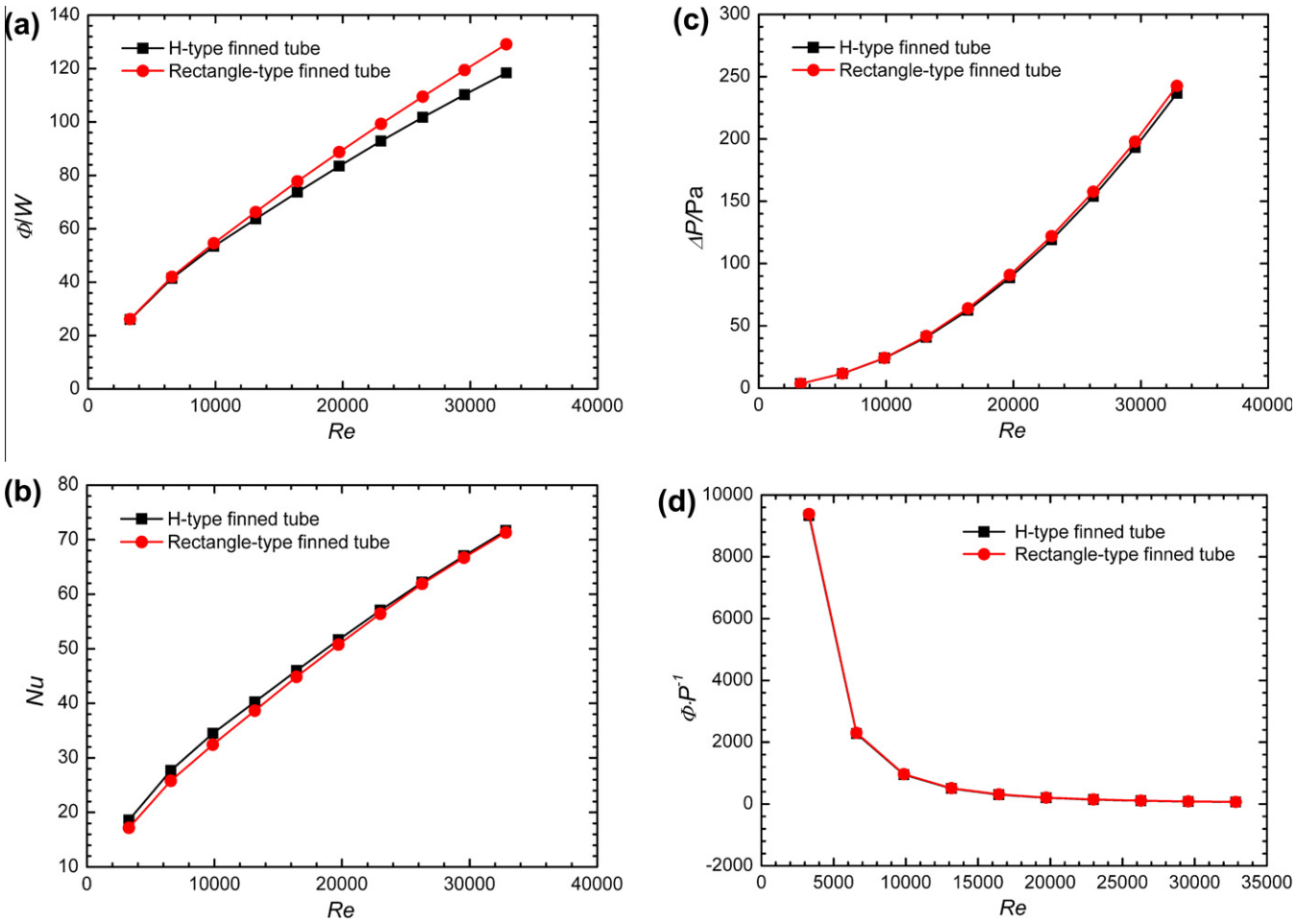

Fig. 4. Variations of heat transfer rate, *Nu*, pressure drop and heat transfer rate per pumping power with *Re* for rectangle-type and H-type finned tube (a) heat transfer rate, (b) *Nu*, (c) pressure drop, (d) heat transfer rate per pumping power.

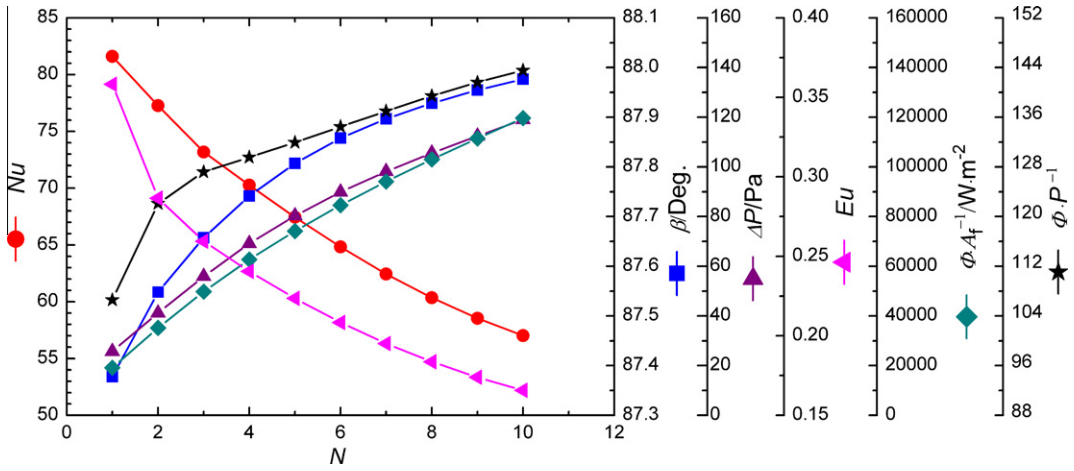

Fig. 5. The effects of number of tube rows on Nusselt number, intersection angle, pressure drop, Euler number, heat transfer rate per unit frontal area and heat transfer rate per pumping power (Re = 15 000).

The variation of tube average Nusselt number for each row of tubes is presented in Fig. 6. It can be seen that the per-tube local Nusselt number decreases with the tube number and approaches a constant when $N \geqslant 9$. The relative difference between the local Nusselt number of tube 9 and 10 is less than 1%, hence when $N \geqslant 10$ the local heat transfer can be regarded as periodically fully developed. This implies that the average heat transfer and pressure drop characteristics obtained in this paper are for the developing region of the tube bundle with 10 streamwise tube rows. Further study is needed to reveal the heat transfer and pressure drop characteristics in the periodically fully developed region. This study has been underway in the authors' group and the results will be reported elsewhere.

In the present study, in order to clarify whether the intersection angles are dependent on the adopted turbulence model, two different models, namely standard $k-\varepsilon$ model and RNG $k-\varepsilon$ model are chosen to simulate the heat transfer and fluid flow of H-type finned tube. The variations of the intersection angle β with the number of tube rows are provided in Fig. 7. It can be seen that these two lines have the same variation tendency and the average intersection angle β obtained by two models are almost identical when $N \geqslant 5$. As indicated in [34], the most important character of the synergy angle is its variation trend, rather than the absolute value. The qualitatively good agreement between the results obtained by two different models shows that the result of field synergy principle analysis is independent on the adopted turbulence model.

3.3. The effect of fin thickness

For examining the effect of fin thickness on the heat transfer and fluid flow, simulations were conducted for the non-dimensional fin thickness from 0.026 to 0.105.

The variations of Nusselt number, intersection angle, pressure drop, heat transfer rate per unit frontal area and heat transfer rate per pumping power with fin thickness are shown in Fig. 8. First, it can be seen that Nu number increases with the increase of fin thickness, while the synergy angle decreases quickly with the increase of fin thickness. Such results are consistent with [30], where the effects of fin thickness on turbulent heat transfer was studied from the view point of FSP. Second, both the pressure drop and the heat transfer rate per unit frontal area increase with the increase of fin thickness. With the increase in fin thickness the average air flow velocity in the fin coil increases, which leads to the increase of heat transfer rate and pressure drop. The heat transfer rate per unit pumping power decreases with the increase of fin thickness. This is because the fact that pressure drop is proportional to $u^{(1.75\sim2.0)}$ while for the convective heat transfer the exponent of velocity is less than 0.8. Therefore, during the design of the H-type finned tube, fin thickness should be made as thin as possible, provided that the heat transfer requirement is met and the manufacturing is realizable.

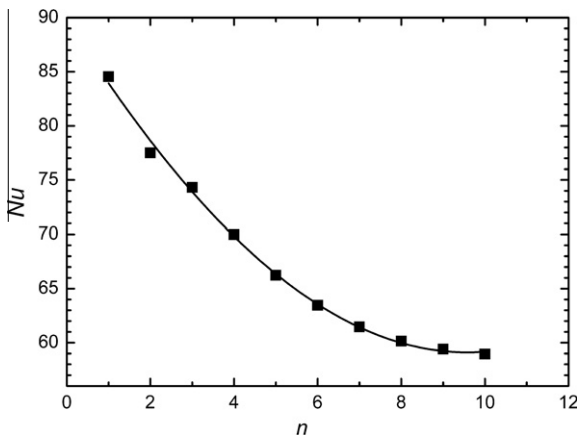

Fig. 6. Nu number of each row of 10-row H-type finned tube.

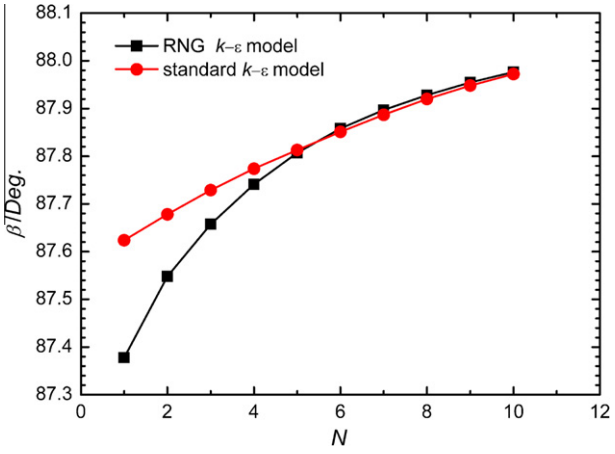

Fig. 7. Variation of the intersection angle β with the number of tube rows.

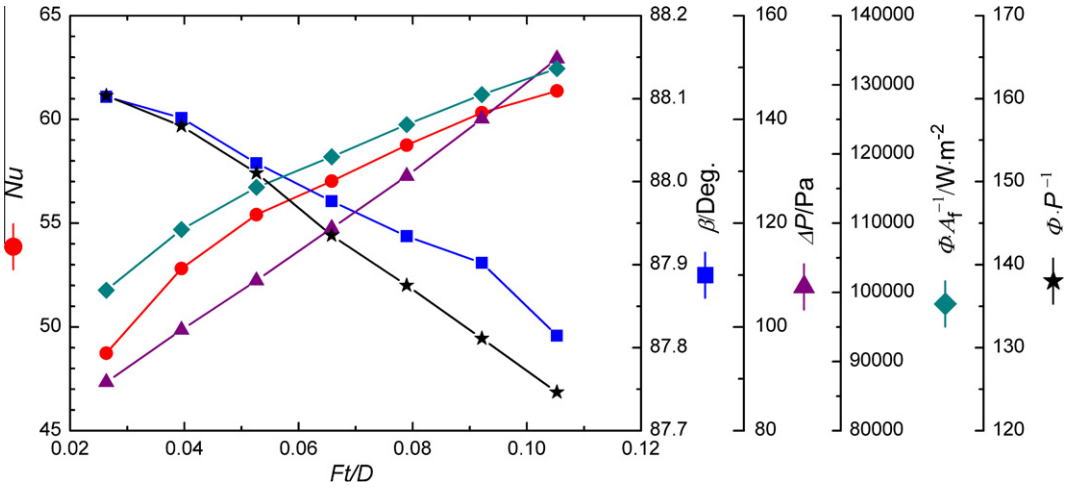

Fig. 8. The effects of fin thickness on Nusselt number, intersection angle, pressure drop, heat transfer rate per unit frontal area and heat transfer rate per pumping power ($N = 10$).

3.4. The effect of slit width

For examining the effect of slit width on the heat transfer and fluid flow, during the simulation the non-dimensional slit width varied from 0.158 to 0.632.

Fig. 9 presents the relations between Nusselt number, intersection angle, pressure drop, heat transfer rate per unit frontal area and heat transfer rate per pumping power and slit width. It can be seen that only the *Nu* number increases with the increase of slit width, while all other parameters decrease with different descending trends. When the slit width is quite narrow, the pressure drop decreases rapidly with its increase. With further increase in the slit width the descending trend of the pressure drop soon becomes mild. As for the synergy angle, heat transfer rate per unit frontal area and heat transfer rate per pumping power, they decrease with the increase in the slot width almost linearly.

3.5. The effect of fin height

The effect of fin height on the heat transfer and pressure drop was examined within a variation range of the non-dimensional fin height from 1.32 to 2.36 during the simulation.

The effects of fin height on Nusselt number, intersection angle, pressure drop, heat transfer rate per unit frontal area and heat transfer rate per pumping power are presented in Fig. 10. Following features may be noted. First, it can be seen that the *Nu* number decreases and the average intersection angle β increases with the increase of fin height, and this is because a longer fin height leads to a higher thickness of the thermal boundary layer. Both the pressure drop and the heat transfer rate per unit frontal area increase with the increase of fin height. The heat transfer area increases with the increase of fin height, which leads to the increase of heat transfer rate and pressure drop. In this paper, T_w is the average temperature of total air side heat transfer area which means that the fin efficiency is implicitly considered in the temperature difference in Eq. (10) from which the heat transfer coefficient is evaluated. Therefore in Eq. (10) A is the total air side heat transfer area (both tube and fin surface). It can be seen that the variation tendency of *Nu* is opposite with that of the pressure drop. The increasing tendency of the heat transfer rate per unit frontal area is larger than that of the pressure drop at first, and then the increasing tendency of the pressure drop is larger than that of the heat transfer rate per unit frontal area. So there exists an optimal fin height (H/D of 1.45) at which the heat transfer rate per unit pumping power is the maximum.

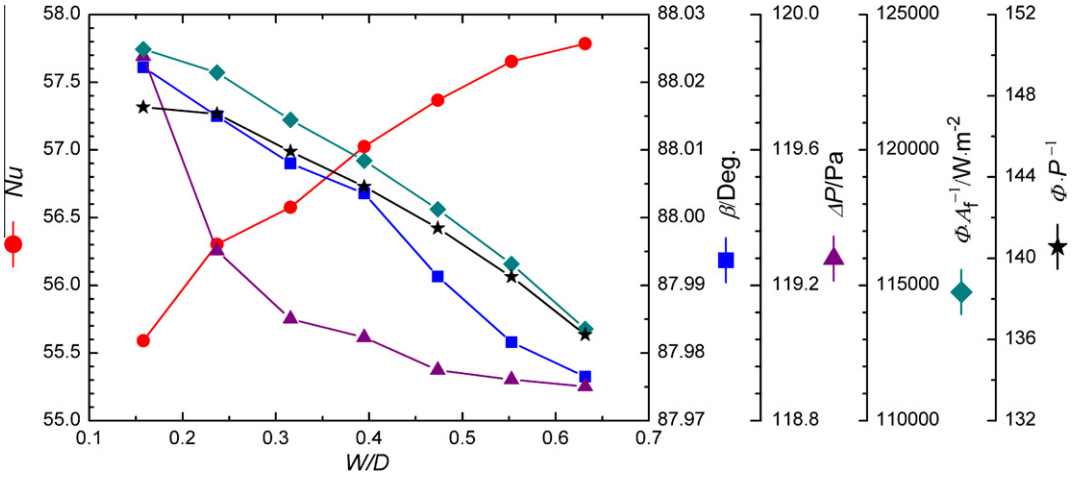

Fig. 9. The effects of slit width on Nusselt number, intersection angle, pressure drop, heat transfer rate per unit frontal area and heat transfer rate per pumping power ($N = 10$).

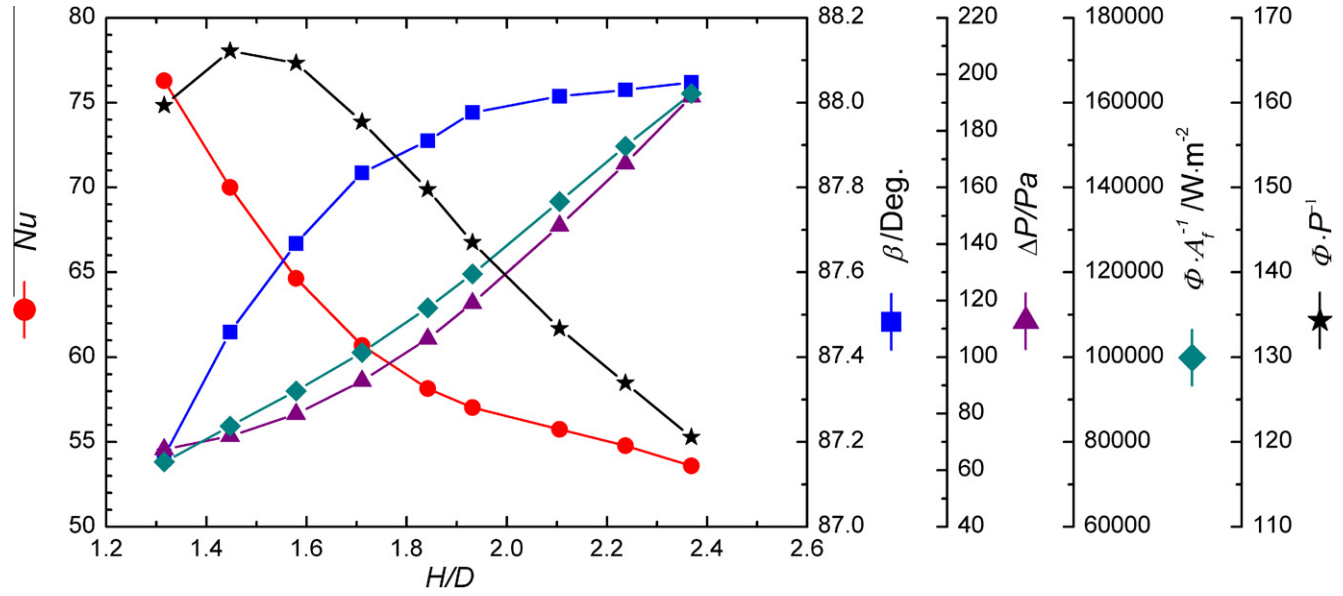

Fig. 10. The effects of fin height on Nusselt number, intersection angle, pressure drop, heat transfer rate per unit frontal area and heat transfer rate per pumping power ($N = 10$).

3.6. The effect of fin pitch

For examining the effect of fin pitch on the heat transfer and fluid flow, during the simulation the non-dimensional fin pitch varied from 0.158 to 0.474.

The relations between Nusselt number, intersection angle, pressure drop, heat transfer rate per unit frontal area and heat transfer rate per pumping power and fin pitch are provided in Fig. 11. It can be seen that the *Nu* number increases with the increase of fin pitch while the average intersection β decreases with the increase of fin pitch. Both the pressure drop and the heat transfer rate per unit frontal area decrease with the increase of fin pitch. The increase of fin pitch leads to lower velocity in the fin coil and less heat transfer surfaces per unit frontal area, leading to a lower pressure drop and heat transfer rate. It should be noted that even though the heat transfer rate per unit frontal area decreases with the increase in fin pitch, the *Nu* number varies in the opposite way. The reason may be explained as follows. The reduction of heat transfer rate with the decrease on velocity is not linear while the reduction of heat transfer surface with the increase in fin pitch is linear, making the heat transfer coefficient being enhanced in somewhat with the increase in fin pitch. The heat transfer rate per unit pumping power increases with the increase of fin pitch and the increasing tendency is weakened gradually. Within the variation range of the fin pitch (from 0.158 to 0.474) the optimal fin pitch in the aspect of pumping power does not exist, but such variation trend can be observed. Therefore, a larger fin pitch of the H-type fin tube surface is in favor of increasing the heat transfer rate per pumping power.

3.7. The effect of spanwise tube pitch

The non-dimensional spanwise tube pitch varied from 2.24 to 3.42 to examine its effect.

The effects of spanwise tube pitch on Nusselt number, intersection angle, pressure drop, heat transfer rate per unit frontal area and heat transfer rate per pumping power are shown in Fig. 12. With the increase of the spanwise tube pitch, the velocity in the fin coil decreases, so both Nusselt number and pressure drop

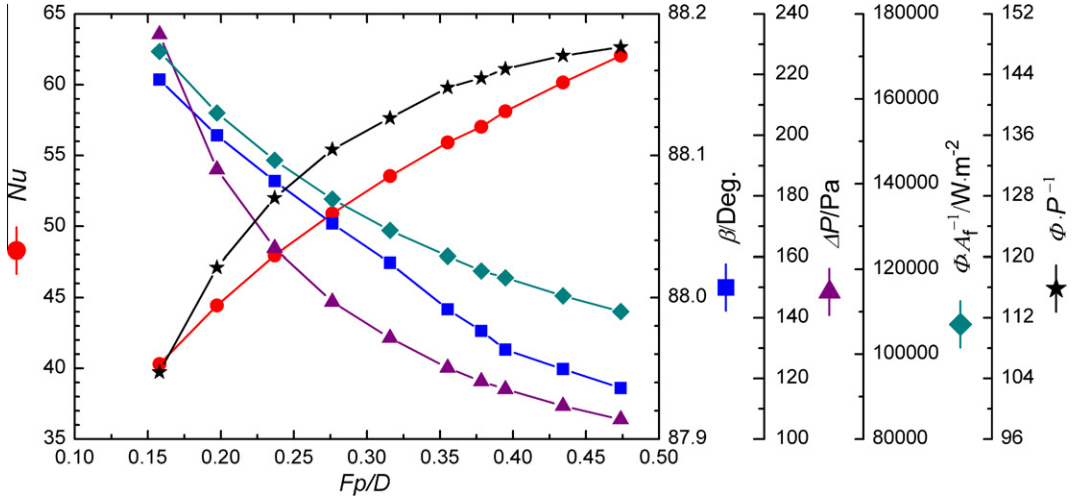

Fig. 11. The effects of fin pitch on Nusselt number, intersection angle, pressure drop, heat transfer rate per unit frontal area and heat transfer rate per pumping power ($N = 10$).

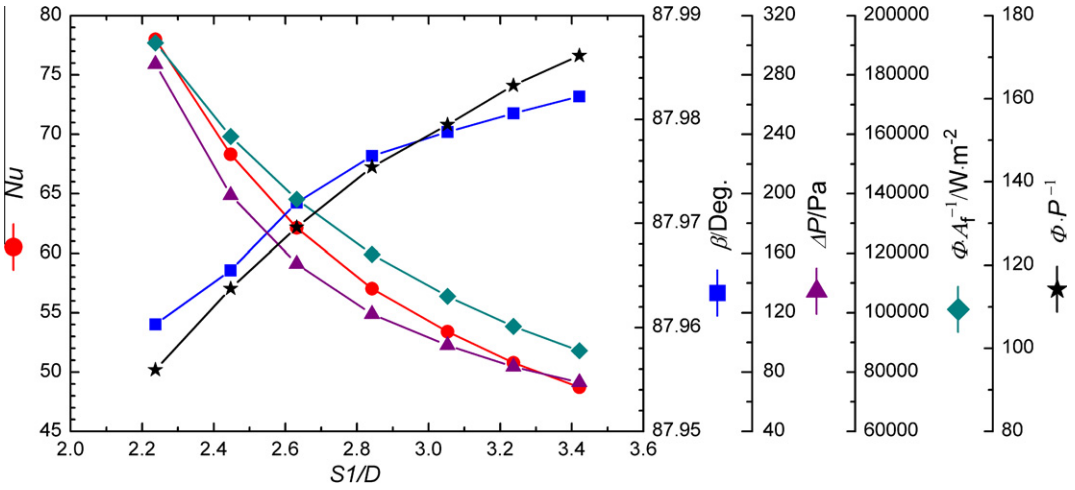

Fig. 12. The effects of spanwise tube pitch on Nusselt number, intersection angle, pressure drop, heat transfer rate per unit frontal area, heat transfer rate per unit volume and heat transfer rate per pumping power ($N = 10$).

decrease, and the synergy angle increases. As indicated before, the dependency of pressure drop on velocity is much stronger than that of heat transfer, hence in the variation range of S_1/D studied, the reduction of *Nu* is only about 38%, while that of pressure drop is as large as 75%. Such variation trends of heat transfer and pressure drop leads to the increase of the heat transfer rate per unit pumping power increases with the spanwise tube pitch.

3.8. The effect of longitudinal tube pitch

The effect of longitudinal tube pitch on the heat transfer and pressure drop was examined within a variation range of the non-dimensional longitudinal tube pitch varied from 2.37 to 3.95 during the simulation.

The effects of longitudinal tube pitch on Nusselt number, intersection angle, pressure drop, heat transfer rate per unit frontal area, heat transfer rate per unit volume and heat transfer rate per pumping power are shown in Fig. 13. It can be seen that *Nu* number increases with the increase of longitudinal tube pitch, while the synergy angle decreases quickly with the increase of longitudinal tube pitch. Both the pressure drop and heat transfer rate per unit frontal area increase with the increase of longitudinal tube pitch. The effect of wake region of the former tube row on the latter row becomes less and less with the increase of the longitudinal tube pitch which leads to a higher velocity of the stream impinging on the tube wall, leading to a higher pressure drop and heat transfer rate. The heat transfer rate per unit volume decreases with the increase of longitudinal tube pitch because of the fact that the heat transfer area per unit volume decreases with the increase of longitudinal tube pitch. In the variation range of S_2/D studied, the growth of heat transfer rate per unit frontal area is about 9%, while that of pressure drop is as large as 18% which leads to the decrease of the heat transfer rate per unit pumping power.

From the above presentation of the effects of seven geometric parameters on the heat transfer and pressure drop characters it can be observed that the most important parameter is spanwise tube pitch, and the least important one is slit width with tube row number, fin thickness, fin height, fin pitch and longitudinal tube pitch in between.

3.9. The effect of Re number

Finally the effect of *Re* number on the heat transfer and pressure drop are examined. For this purpose simulations were performed for the inlet velocity from 1 to 10 m/s, corresponding to a variation

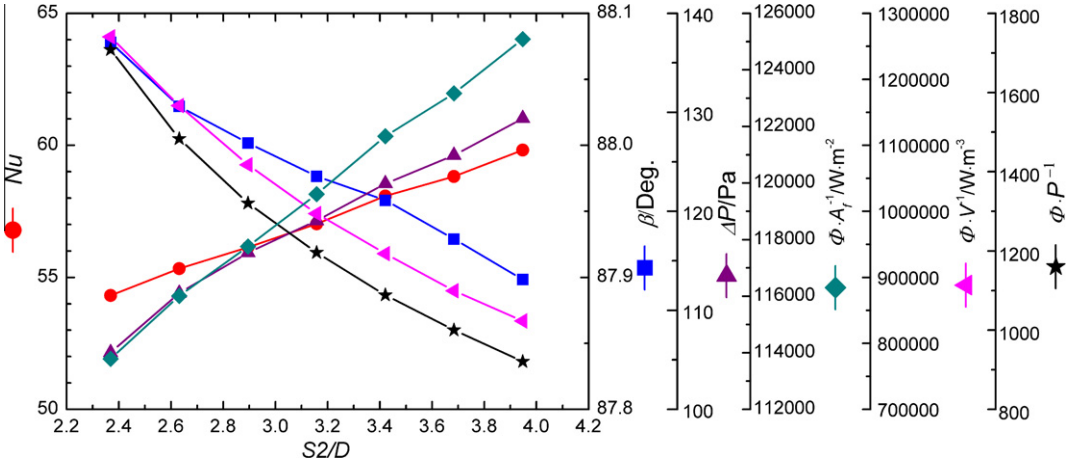

Fig. 13. The effects of longitudinal tube pitch on Nusselt number, intersection angle, pressure drop, heat transfer rate per unit frontal area, heat transfer rate per unit volume and heat transfer rate per pumping power ($N = 10$).

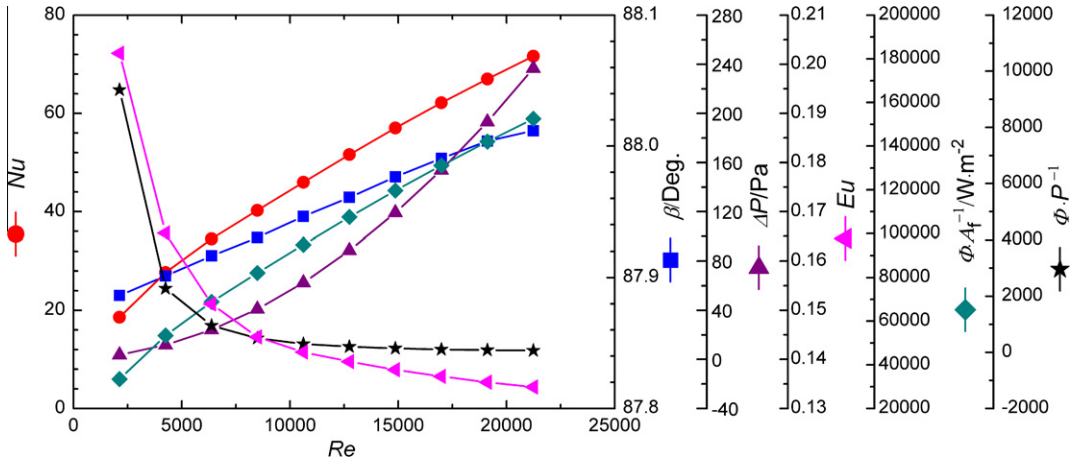

Fig. 14. The effects of *Re* number on Nusselt number, intersection angle, pressure drop, Euler number, heat transfer rate per unit frontal area and heat transfer rate per pumping power ($N = 10$).

range of *Re* from 2.1×10^3 to 2.1×10^4. The other parameters remained the same.

Fig. 14 shows the variations of Nusselt number, intersection angle, pressure drop, Euler number, heat transfer rate per unit frontal area and heat transfer rate per pumping power with *Re*. The variation trends of all the six parameters with *Re* are expectable with following two features worth further mentioning. First, the average intersection angle β increases with the increase of *Re*, which implies the deterioration of the synergy between the temperature gradient and velocity with *Re*. For an angle as large as 88 degree, a minor change in the angle will result in an appreciable difference in cosine, and this result agrees with all previous works [11–17]. Second, the stronger dependence of pressure drop with velocity than that of *Nu* leads to a descending variation of the heat transfer rate per unit pumping power decreases with *Re*. However, when *Re* is larger than 10000, this parameter almost remains constant. Thus the inlet velocity is an essential factor affecting the comprehensive performance of the H-type finned tube heat exchanger.

4. Multiple correlation

Based on the above series of parametric computations, it is not sufficient to end up only with the numerical results, but the data of heat transfer and pressure drop should be compressed in compact forms so that some practical correlations can be obtained. According to the similarity theory [35] the following correlation forms are assumed:

$$Nu = C_1 Re^{C_2} \left(\frac{F_p}{D}\right)^{C_3} \left(\frac{F_t}{D}\right)^{C_4} \left(\frac{S_1}{D}\right)^{C_5} \left(\frac{S_2}{D}\right)^{C_6} \left(\frac{H}{D}\right)^{C_7} \left(\frac{W}{D}\right)^{C_8} \quad (16)$$

$$Eu = C_1 Re^{C_2} \left(\frac{F_p}{D}\right)^{C_3} \left(\frac{F_t}{D}\right)^{C_4} \left(\frac{S_1}{D}\right)^{C_5} \left(\frac{S_2}{D}\right)^{C_6} \left(\frac{H}{D}\right)^{C_7} \left(\frac{W}{D}\right)^{C_8} \quad (17)$$

The eight coefficients C_1, C_2, C_3, C_4, C_5, C_6, C_7, and C_8 should be determined by means of multiple regression technique [36]. The final results are as follows:

$$Nu = 1.66 Re^{0.585} \left(\frac{F_p}{D}\right)^{0.389} \left(\frac{F_t}{D}\right)^{0.165} \left(\frac{S_1}{D}\right)^{-1.108} \left(\frac{S_2}{D}\right)^{0.293} \left(\frac{H}{D}\right)^{-0.624} \left(\frac{W}{D}\right)^{0.029} \quad (18)$$

$$Eu = 11.63 Re^{-0.157} \left(\frac{F_p}{D}\right)^{-0.693} \left(\frac{F_t}{D}\right)^{0.375} \left(\frac{S_1}{D}\right)^{-3.026} \left(\frac{S_2}{D}\right)^{-0.388} \left(\frac{H}{D}\right)^{1.835} \left(\frac{W}{D}\right)^{-0.002} \quad (19)$$

The predicted results from the correlations and original data are compared in Fig. 15. All of the deviations but one is within 10% and the average deviation being around 2.3%, indicating that the correlations are of sufficient accuracy. The application ranges of the present correlations are listed as follow:

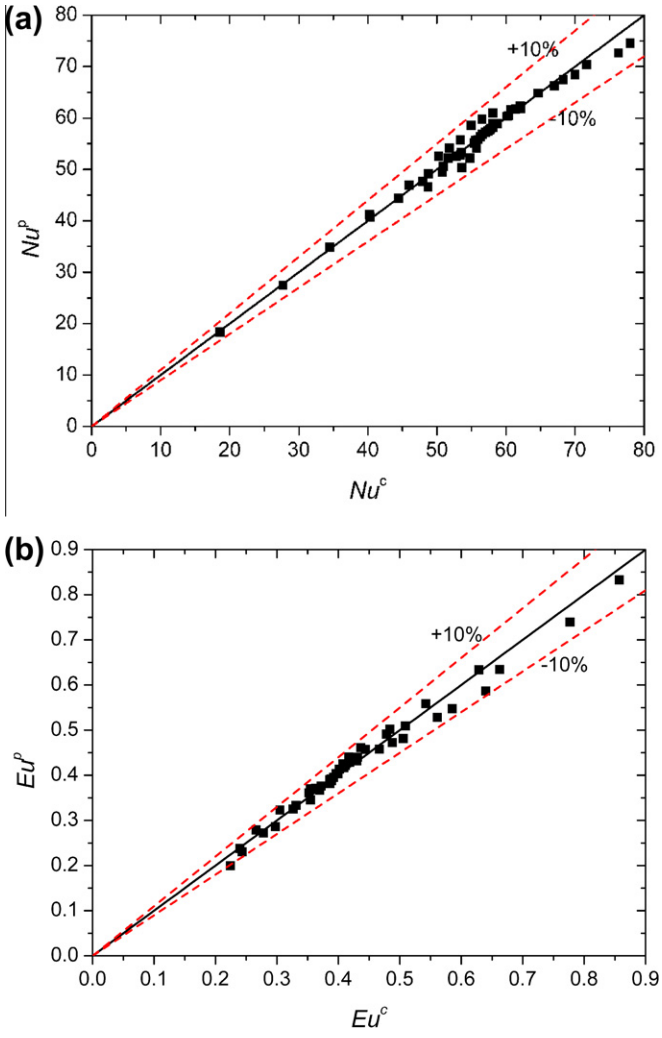

Fig. 15. Comparison between predicted results and numerical data (a) *Nu* and (b) *Eu*.

$Re = 2100–21000$, $D = 38$ mm, $F_p/D = 0.158–0.474$, $F_t/D = 0.026–0.105$, $S_1/D = 2.24–3.42$, $S_2/D = 2.37–3.95$, $H/D = 1.32–2.36$, $W/D = 0.158–0.632$.

It is worth noting that Eqs. (18) and (19) provide the averaged characteristics of heat transfer and pressure drop of the H-type finned tube bank of 10 rows. As a whole, the fluid flow and heat transfer in the bank are in the developing region. Further study is needed to obtain the heat transfer and pressure drop characteristics of the H-type finned tube bank for the fully developed region.

5. Conclusion

In this paper, three-dimensional numerical studies were performed for heat transfer and fluid flow characteristics of H-type finned tube bank with 10 rows of tubes by software FLUENT. The following conclusions can be made.

1. Among the seven geometric parameters spanwise tube pitch has the most important effect and slit width has the least important effect, with other five parameters in between.
2. The per-tube local Nusselt number decreases with the tube number and approaches a constant when $N \geqslant 9$. When $N \geqslant 10$ the local heat transfer can be regarded as periodically fully developed.
3. The variation trends of *Nu* with the eight parameters are in good agreement with the field synergy principle.
4. The numerical data for *Nu* and *Eu* can be well correlated by Eqs. (18) and (19), respectively, which may be useful to engineering design for clean gas situation.

Acknowledgments

We gratefully acknowledge the support of this work by the National Basic Research Program of China (973 Program, No. 2013CB228304, 2011CB710702) and thank doctorate students Li Chen, Zhi-Qiang Yu, Zhao-Hui Li, Hu Zhang, and Ming-Jie Li for their assistance in this study.

References

[1] C.C. Wang, W.L. Fu, C.T. Chang, Heat transfer and friction characteristics of typical wavy fin-and-tube heat exchangers, Exp. Thermal Fluid Sci. 14 (2) (1997) 174–186.
[2] C.C. Wang, J.Y. Chang, N.F. Chiou, Effects of waffle height on the air-side performance of wavy fin-and-tube heat exchangers, Heat Transfer Eng. 20 (3) (1999) 45–56.
[3] C.C. Wang, J.Y. Jang, N.F. Chiou, A heat transfer and friction correlation for wavy fin-and-tube heat exchangers, Int. J. Heat Mass Transfer 42 (10) (1999) 1919–1924.
[4] C.C. Wang, W.H. Tao, Y.J. Du, Effect of waffle height on the air-side performance of wavy fin-and-tube heat exchangers under dehumidifying conditions, Heat Transfer Eng. 21 (5) (2000) 17–26.
[5] C.C. Wang, Y.M. Hwang, Y.T. Lin, Empirical correlations for heat transfer and flow friction characteristics of herringbone wavy fin-and-tube heat exchangers, Int. J. Refrig. – Rev. Int. Du Froid 25 (5) (2002) 673–680.
[6] C.C. Wang, J.S. Liaw, B.C. Yang, Airside performance of herringbone wavy fin-and-tube heat exchangers – data with larger diameter tube, Int. J. Heat Mass Transfer 54 (5–6) (2011) 1024–1029.
[7] M. Abu Madi, R.A. Johns, M.R. Heikal, Performance characteristics correlation for round tube and plate finned heat exchangers, Int. J. Refrig. – Rev. Int. Du Froid 21 (7) (1998) 507–517.
[8] F. Halici, I. Taymaz, M. Gunduz, The effect of the number of tube rows on heat, mass and momentum transfer in flat-plate finned tube heat exchangers, Energy 26 (11) (2001) 963–972.
[9] G. Lozza, U. Merlo, An experimental investigation of heat transfer and friction losses of interrupted and wavy fins for fin-and-tube heat exchangers, Int. J. Refrig. – Rev. Int. Du Froid 24 (5) (2001) 409–416.
[10] M.S. Mon, U. Gross, Numerical study of fin-spacing effects in annular-finned tube heat exchangers, Int. J. Heat Mass Transfer 47 (8–9) (2004) 1953–1964.
[11] Y.P. Cheng, Z.G. Qu, W.Q. Tao, Y.L. He, Numerical design of efficient slotted fin surface based on the field synergy principle, Numer. Heat Transfer, Part A 45 (6) (2004) 517–538.
[12] Z.G. Qu, W.Q. Tao, Y.L. He, Three dimensional numerical simulation on laminar heat transfer and fluid flow characteristics of strip fin surfaces with X-arrangement of strips, ASME J. Heat Transfer 126 (4) (2004) 697–707.
[13] Y.L. He, W.Q. Tao, F.Q. Song, W. Zhang, Three-dimensional numerical study of heat transfer characteristics of plain plate fin-and-tube heat exchangers from view point of field synergy principle, Int. J. Heat Fluid Flow 26 (3) (2005) 459–473.
[14] J.J. Zhou, W.Q. Tao, Three-dimensional numerical simulation and analysis of the airside performance of slotted fin surfaces with radial strips, Eng. Comput. 22 (7/8) (2005) 940–957.
[15] W.Q. Tao, W.W. Jin, Y.L. He, Z.G. Qu, C.C. Zhang, Optimum design of two-row slotted fin surface with X-shape strip arrangement positioned by "Front Coarse and Rear Dense" principle, Part 1: physical and mathematical models and numerical methods, Numer. Heat Transfer, Part B 50 (8) (2006) 731–750.
[16] W.W. Jin, Y.L. He, Z.G. Qu, C.C. Zhang, W.Q. Tao, Optimum design of two-row slotted fin surface with X-shape strip arrangement positioned by "Front Coarse and Rear Dense" principle, Part 2: results and discussion, Numer. Heat Transfer, Part B, Part A 50 (8) (2006) 751–772.
[17] Y.B. Tao, Y.L. He, Z.G. Wu, W.Q. Tao, Three-dimensional numerical study and field synergy principle analysis of wavy fin heat exchangers with elliptic tubes, Int. J. Heat Fluid Flow 28 (6) (2007) 1531–1544.
[18] G.N. Xie, Q.W. Wang, B. Sunden, Parametric study and multiple correlations on air-side heat transfer and friction characteristics of fin-and-tube heat exchangers with large number of large-diameter tube rows, Appl. Therm. Eng. 29 (1) (2009) 1–16.
[19] Y.Z. Liu, Y.C. Yuan, S.Y. Xu, W.B. Wu, Experimental study on the characteristics of heat transfer and flow resistance for H-type finned tube banks, J. Univ. Shanghai Sci. Technol. 26 (5) (2004) 457–460.
[20] X.N. Yu, Y.C. Yuan, Y.F. Ma, H.L. Liu, Experimental tests and numerical simulation on heat transfer and resistance characteristics of H-type finned tube banks, J. Chin. Soc. Power Eng. 30 (6) (2010) 433–438.
[21] Z.X. Zhang, Y.G. Wang, Q.X. Zhao, Numerical simulation and verification on heat transfer characteristics of H-type finned tubes, J. Chin. Soc. Power Eng. 30 (5) (2010) 368–371.
[22] Z.Y. Guo, D.Y. Li, B.X. Wang, A novel concept for convective heat transfer enhancement, Int. J. Heat Mass Transfer 41 (14) (1998) 2221–2225.
[23] Z.Y. Guo, W.Q. Tao, R.K. Shah, The field synergy (coordination) principle and its applications in enhancing single phase convective heat transfer, Int. J. Heat Mass Transfer 48 (9) (2005) 1797–1807.
[24] Z.G. Qu, W.Q. Tao, Y.L. He, Three-dimensional numerical simulation on laminar heat transfer and fluid flow characteristics of strip fin surface with x-arrangement of strips, J. Heat Transfer – Trans. ASME 126 (5) (2004) 697–707.
[25] S. Shen, W. Liu, W.Q. Tao, Analysis of field synergy on natural convective heat transfer in porous media, Int. Commun. Heat Mass Transfer 30 (8) (2003) 1081–1090.
[26] W.Q. Tao, Z.Y. Guo, B.X. Wang, Field synergy principle for enhancing convective heat transfer – its extension and numerical verifications, Int. J. Heat Mass Transfer 45 (18) (2002) 3849–3856.
[27] W.Q. Tao, Y.L. He, Z.G. Qu, Y.P. Cheng, Applications of the field synergy principle in developing new type heat transfer enhanced surfaces, J. Enhanced Heat Transfer 11 (4) (2004) 435–451.
[28] W.Q. Tao, Y.L. He, Q.W. Wang, Z.G. Qu, F.Q. Song, A unified analysis on enhancing single phase convective heat transfer with field synergy principle, Int. J. Heat Mass Transfer 45 (24) (2002) 4871–4879.
[29] J.M. Wu, W.Q. Tao, Investigation on laminar convection heat transfer in fin-and-tube heat exchanger in aligned arrangement with longitudinal vortex generator from the viewpoint of field synergy principle, Appl. Therm. Eng. 27 (14–15) (2007) 2609–2617.
[30] M. Zeng, W.Q. Tao, Numerical verification of the field synergy principle for turbulent flow, J. Enhanced Heat Transfer 11 (4) (2004) 453–459.
[31] W.Q. Tao, Numerical Heat Transfer, second ed., Xi'an Jiaotong University Press, Xi'an, China, 2001.
[32] V. Yakhot, S.A. Orszag, Renormalization group analysis of turbulence. I. Basic theory, J. Sci. Comput. 1 (1) (1986) 7–20.
[33] F. Incorporated, Fluent 6.2 User's Guide, in: Fluent Incorporated Lebanon, NH, USA, 2004.
[34] J.J. Zhou, Research on the Mechanisms of Heat Transfer Enhancement and Saving Energy for Compact Heat Exchanger Surfaces and Its Optimization (Desertation), Xi'an Jiaotong Univesity, Xi'an, China, 2005.
[35] S.M. Yang, W.Q. Tao, Heat Transfer, fourth ed., Higher Education Press, Beijing, China, 2006.
[36] J.G. Orme, T. Combs-Orme, Multiple Regression with Discrete Dependent Variables, Oxford University Press, New York, USA, 2009.